Postprint Version

G. McHale, N.J. Shirtcliffe, M.I. Newton and F.B. Pyatt, *Implications of ideas on super-hydrophobicity for water repellent soil*, Hydrol. Proc. 21 (17) (2007) 2229-2238; DOI:10.1002/hyp.6765.

Implications of ideas on super-hydrophobicity for water repellent soil

G. MCHALE, N.J. SHIRTCLIFFE, M.I. NEWTON AND F.B. PYATT

School of Biomedical & Natural Sciences, Nottingham Trent University, Clifton Lane, Nottingham NG11 8NS, UK

Correspondence: G. McHale. E-mail: glen.mchale@ntu.ac.uk

Abstract

Water repellence is an important factor in soil erosion due to its role in inhibiting the re-establishment of vegetation after fire and due to its enhancement of run-off. Water repellence is studied across a range of diverse disciplines, such as chemistry, materials, textiles and soil and reclamation science. In recent years many basic studies of water repellence of materials have focused on the role of the sub-mm surface topography of a material in modifying the intrinsic hydrophobicity imparted by the surface chemistry to create super-hydrophobicity. In this report, we first illustrate the types of hydrophobic effects created by a suitable coupling of small scale surface topography with surface chemistry using three examples of materials: an etched metal, a foam and a micro-fabricated pillar structure. These examples demonstrate the general applicability of the ideas and suggest that they could apply to a granular material, such as a fine sandy soil, particularly when the grains have become coated with a hydrophobic layer. This applicability is confirmed by contact angle measurements of droplets of water on hydrophobic sand. A theoretical model describing the application of these ideas to a loose-packed, but regular, array of uniform spherical grains is then presented and discussed. When the grains are in a dry initial state the effect of the surface is to increase the apparent water repellence as observed through the contact angle. However, when the spaces between the grains are initially filled with water, the effect is to provide greater wetting. To qualitatively confirm the enhancement of contact angle caused by the granular structure, model surfaces using 600 μm and 250 μm hydrophobic glass beads were created. On these surfaces, the contact angle of droplets of water was increased from 108^{o} to 126^{o} and 140^{o}, respectively.

Keywords: Water repellence; Contact angle; Hydrophobic; Superhydrophobic.

INTRODUCTION

Enhanced or extreme water repellence can occur after fire or intense heating of soil containing hydrophobic organic matter (DeBano, 2000; Letey, 2001), after contamination of land during oil or other spillages (Roy and McGill, 1998, 2002) or naturally under certain vegetation types. Such enhancement of water repellence has far reaching implications such as increased soil erosion due to accelerated run-off, enhanced preferential flow and reduced vegetation growth in the affected ecosystem (Doerr *et al*., 2003; Terry and Shakesby, 1993; Karnok *et al*., 1993). Understanding water repellence is not restricted to soil science, but is a common concern across many scientific and engineering problems including textiles, materials and building construction. However, the language and techniques used to investigate and describe similar aspects of these problems are often different and translating common issues and progress between one discipline and another, quite disparate, discipline can be difficult.

In physical chemistry, hydrophobicity originates from the surface chemistry and is often investigated using contact angle measurements (Adamson and Gast, 1997). A fundamental concept is the contact angle, θ_e, on a smooth solid predicted theoretically by Young's law,

$$\cos\theta_e = (\gamma_{SV} - \gamma_{SL})/\gamma_{LV} \qquad (1)$$

where the γ_{ij} are the various interfacial tensions between the solid, vapor and liquid; the Young's law contact angle θ_e summarizes the chemistry (or intrinsic hydrophobicity) of the solid-liquid-vapor system. However, in textiles the shape and weave of fibers can be as important as the precise surface chemistry and the use of contact angles is often replaced by water drop penetration time (WDPT) tests. In soil studies, water drop penetration time (WDPT) and molarity of ethanol droplet (MED) tests are used widely (Doerr, 1998; Roy and McGill, 2002; Van't Woudt, 1959), whereas within materials work, contact angle studies are common. The differences in techniques deployed are necessitated by the need for *in-situ* fieldwork and the potential ambiguities that occur when field samples are prepared for laboratory work or when idealized models are created in the laboratory. However, the differences in language and techniques also indicate an underlying difference in emphasis between surface chemistry and the small scale surface shape or topography.

In this report we focus on how the coupling of the surface chemistry of a material with the sub-mm topography of a surface can create extreme water repellence; an effect often referred to as super-hydrophobicity. Our aim is to provide an understanding of the application of concepts from materials science to a granular material, such as a loose sandy soil. We do not claim or imply we are experts in soil science, but rather we provide three examples of materials and experiments from our laboratory that illustrate the relationship between sub-mm topography and extreme water repellence. The first example uses etched and non-etched metal surfaces with the same surface chemistry to develop the role of topography in enhancing wetting (Shirtcliffe *et al*., 2005a). The second example is a foam and is used to develop an

understanding of the role of surface chemistry in a converting a given structure to a super-hydrophobic material (Shirtcliffe *et al*., 2003; Shirtcliffe *et al*., 2005b). The third example, uses a microfabricated pillar system to show that super-hydrophobicity can be quantitatively described and that the exact influence of topography depends upon the aspect ratio of features and not simply surface roughness (Shirtcliffe *et al*., 2004). These examples have previously been published as specific methods of creating super-hydrophobic surfaces, but are used here to develop a coherent and systematic view of general principles that we believe are relevant to a hydrophobic granular surface as found in soil science. Such a surface could be produced during a wildfire by the volatilization of organic compounds and their re-condensation onto suitable size and shape grains within the soil profile.

To further investigate the implications of previous quantitative modeling of a hydrophobic granular surface (McHale *et al.*, 2005), we extend the model to examine the effect of relaxing the condition of close-packing of spherical grains. We show how topographic enhancement of hydrophobicity to super-hydrophobicity can collapse depending upon the combination of grain spacing and degree of intrinsic hydrophobicity of the solid. We discuss the limitations on validity of the model due to the fact that grains of soil may not be fixed, but can be lifted from the surface. We also present new data for experiments with surfaces composed of hydrophobized glass beads and sand. Thus, while a major focus of this article is to develop the underlying concepts of super-hydrophobic materials in a manner relevant to soil water repellency, it also provides evidence for super-hydrophobic effects in soil water repellency and limitations on their applicability. In particular, these effects could provide a mechanism for enhancement of soil water repellence through the relative size and spacing of grains and pores and a possible explanation for why soil water repellence should be more prevalent under dry conditions than wet.

MATERIALS SCIENCE EXPERIMENTS

Role of topography

One extreme of the topography-hydrophobicity relationship is a smooth surface with either its intrinsic chemical functionality or with a hydrophobic coating. Figure 1a shows a droplet of water of approximately 2 mm diameter on a smooth copper surface and Figure 1b shows a droplet on a smooth copper surface after it has been treated with a fluorocarbon based water repellent treatment (Grangers extreme wash-in solution designed for re-waterproofing Goretex jackets); the droplet, together with its reflection in the surface, is shown in side-profile and silhouetted using back-lighting. The change in the surface chemistry seen by the droplet of water results in an increase in the contact angle, the angle tangent to the water-air interface measured at the point of contact with the solid surface, towards 110-120^{o}. Increasing a contact angle above 120^{o} purely by the use of surface chemistry is difficult. The other extreme of the topography-hydrophobicity relationship is shown in Figure 1c. In this experiment, we etched a series of craters, of approximately 25 µm diameter, in a square lattice array, in the copper surface prior to treating the surface with the hydrophobizing solution (Shirtcliffe *et al*., 2005a). In fact, in this experiment the

craters were over-etched until the craters joined and left a regular array of pinnacles approximately 50 µm apart. The image shows a contact angle in excess of 160°, which is higher than the 150°, which is usually taken as the formal definition of a super-hydrophobic surface (for a review of such surfaces see Blossey, 2003 and references therein).

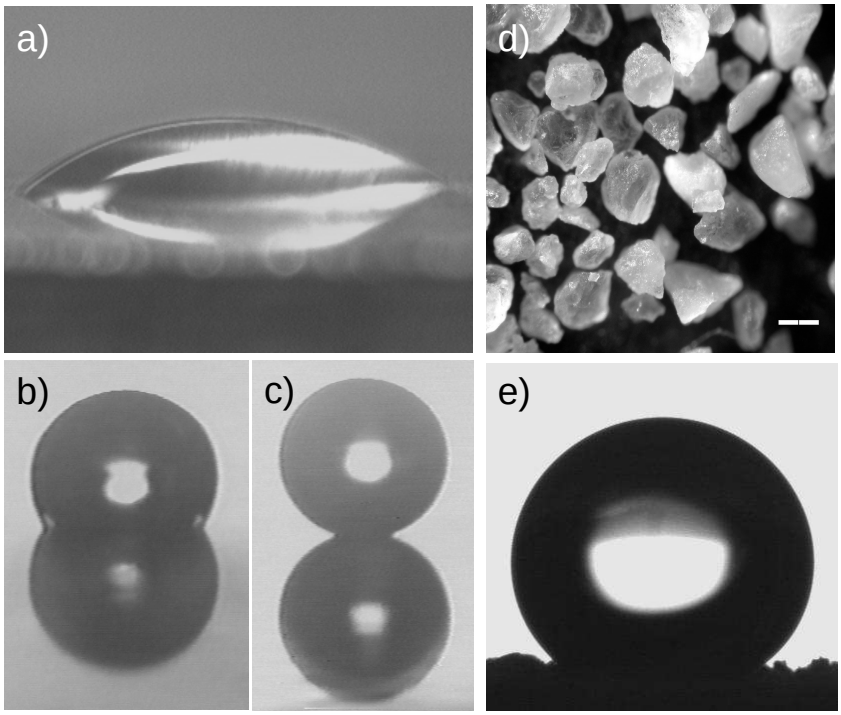

Figure 1 Side view profiles of water droplets and their reflections on (a) a flat copper surface, (b) a flat hydrophobic copper surface, and (c) a hydrophobized etched copper surface. Panel (d) shows the packing and density of a surface composed of hydrophobic sand (scale bar is 200 µm), and (e) shows a droplet of water (contact angle of 139°) on the surface in (d).

The interpretation of the water droplet in Figure 1c is that it is suspended on the peaks of the surface topography and bridges across the gaps. This is possible because the length scales are such to make surface tension, γ_{LV}, rather than gravity, the dominant force. A simple estimate of the length scale for capillarity to dominate is given by the capillary length $\kappa^{-1}=(\gamma_{LV}/\rho g)^{1/2}$. The origins of this can be seen by comparing the weight of a spherical droplet, $4\pi\rho R^3/3$, where ρ is density and R is the spherical radius, with a typical surface tension force of $2\pi R\gamma_{LV}$. For water the capillary length is 2.7 mm and so water on surfaces with length scales of around 270 µm and less will be surface tension dominated. In experiments, such as Figure 1c, feature separations of 50 µm have been shown to produce super-hydrophobic effects; larger separations may also do so, but we have not shown this systematically. Surfaces created by etching copper may not initially appear similar to soil, but the key features of sharp pinnacles with a suitable separation and a hydrophobic surface chemistry is relevant to grains of sand possessing a hydrophobic coating (Figure 1d and 1e). In Figure 1e, the droplet sits within a slight depression and the actual contact angle of around 139°, suggests that the shape and packing of the sand grains may play a role

analogous to surface topography. The experiments with etched copper surfaces show that surface chemistry alone is not sufficient to create extreme water repellence; the small scale surface topography also needs to be suitable and it can certainly be in the size range of fine sand.

Role of Chemistry

Another quite different material we have made in our laboratory is a porous methyl terminated sol-gel glass (MTEOS sol-gel) (Shirtcliffe *et al*., 2003). Without the hydrophobic outward facing methyl groups, this material is a crumbly foam that acts like a sponge. However, with the methyl groups facing outwards, a droplet of water is unable to enter the pores and a droplet of water sits upon the surface protrusions skating across the pores in-between. Figure 2a shows a droplet of water (with some food coloring to provide contrast) on the MTEOS foam which appears white. When the drop is removed the foam remains unstained indicating that there was no penetration of the water into the surface. However, if we heat this particular foam to above 400 ^{o}C and cool it again, then we remove the hydrophobic surface chemistry with little change to the physical structure of the foam (Figure 2c). The effect on the water repellence is immediately obvious - when we deposit a droplet of water on its surface, the foam imbibes all of the liquid and the foam now acts as a super-sponge (Shirtcliffe *et al*., 2005b). The extreme water repellence of such a heat-treated foam can be re-established by treating it with a hydrophobizing solution. The pores in these foams can be tailored to be of the size of tens of nanometers to tens of microns. These experiments show that a porous material can provide a suitable small scale surface topography for extreme water repellence, but that suitable surface chemistry is still required for it to be observed. They also show that a suitable surface or material can be switched between super-hydrophobic and water-imbibing and back again by changing the surface chemistry, and that the precise surface chemistry is not an issue provided it imparts sufficient hydrophobicity to the small scale surface topography.

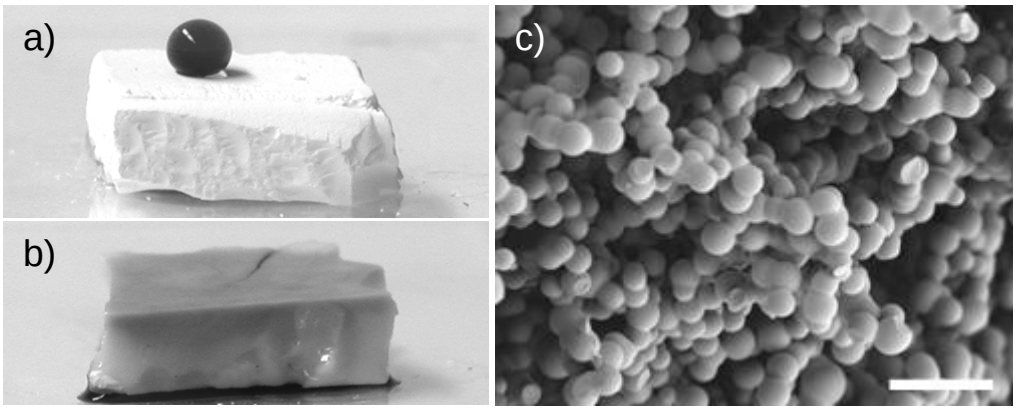

Figure 2 Skating-to-penetrating transition on a hydrophobic foam. (a) Droplet of water with some food coloring on an MTEOS sol-gel, (b) same sol-gel, but after heat treatment to remove the hydrophobic surface functional groups: the droplet of water completely penetrates and stains the foam. (c) the pore structure of the sol-gel used in (a) and (b) (scale bar is 10 μm).

Skating-to-Penetrating Transition

The sol-gel foam material shows a transition from a water droplet penetrating material to a water droplet skating across the surface protrusions of the material dependent upon the surface chemistry of the foam. This concept of penetration-to-skating can be investigated systematically using a microfabricated surface consisting of a regular array of pillars (Shirtcliffe *et al.*, 2004). In Figure 3 the contact angle for a water droplet is shown as the height of the pillars is increased; the inset shows a scanning electron microscope image of the surface. The pillars are circular in cross-section with a 15 µm diameter and arranged in a square array with centre-centre separation of 30 µm and are made using a polymer material (SU-8), which is strong, hard and chemically resistant. For a flat surface of this polymer the contact angle is around 80^o, but as surfaces are constructed with successively taller pillars a sudden transition to a contact angle of above 140^o occurs. This higher contact angle is due to the water droplet no longer penetrating between the pillars. Once the droplet skates across the top of the pillars, bridging the gaps in-between, the droplet effectively sits on a composite surface consisting of the pillar tops and the air gaps between pillar tops. This simple view immediately provides quantitative predictions consistent with the experiments (Cassie and Baxter, 1944). Considering the plane of the tops of the pillars, the basic unit used to create the pattern of pillars has one circle of radius r_p within a square of side lengths $4r_p$ thus giving a basic unit area equal to 16 r_p^2 of which the solid surface area is πr_p^2. The planar fraction of solid surface area at the tops of the pillars is therefore $f = \pi/16 = 0.196$ and the air fraction is $(1-f) = 0.804$. The cosine of the observed contact angle, $\cos\theta_o$, is a weighted sum of the contact angle on the solid (i.e. 80^o) and the contact angle on air (i.e. 180^o because a droplet of water in air completely balls up into a sphere), i.e. $\cos\theta_o = 0.196 \cos(80^o) + 0.804 \cos(180^o)$, which gives the observed contact angle of $\theta_o = 140^o$. These experiments show that relatively simple views of the combination of small scale surface topography and the surface chemistry can be used to make quantitative predictions about extreme water repellence if the water droplets are in the skating regime.

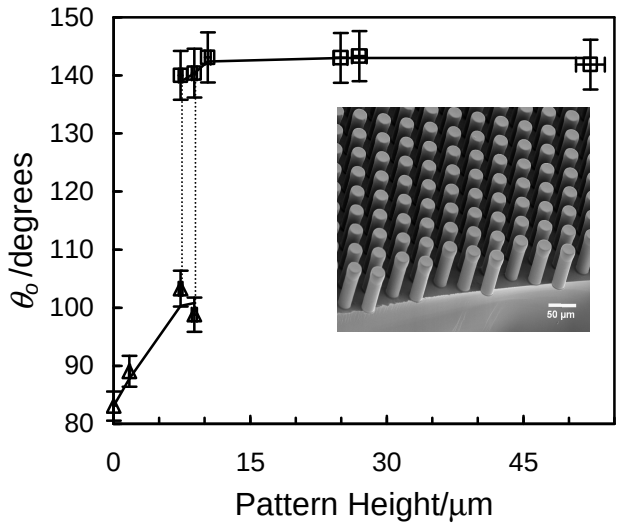

Figure 3 Observed contact angle, θ_o, for a water droplet on square lattices of polymer pillars of diameter 15 µm and centre-to-centre separation of 30 µm and various heights; the surface has been treated with a hydrophobic coating. The inset shows an SEM image of the surface.

Role of Roughness

The pillar surface illustrates that once a droplet skates across surface protrusions, the observed water repellence is a combination of surface chemistry via the intrinsic contact angle, θ_e, on the solid and surface topography via the solid fraction f. Indeed, once a minimum height of pillars has been achieved and skating has occurred (i.e. there is no capillary penetration) the height of the pillars is no longer an influence on the observed contact angle. This means that the roughness factor, r, defined as the ratio of true solid surface area to the horizontally projected surface area is not a relevant parameter for a droplet skating across protrusions. For the circular profile pillars of radius r_p arranged in a square pattern with repeat lengths of 2 r_p, the roughness is a function of pillar height, h_p, and is $r=(16\ r_p^2+2\pi r_p h_p)/\ 16\ r_p^2 = 1 + 0.393 h_p/r_p$. Whilst the roughness factor is not a relevant parameter once the water droplet enters the skating regime, it is relevant if the liquid penetrates between surface features. Figure 4 shows results for droplets of different liquids placed upon the pillar surface. The horizontal axis shows the contact angle measured on a flat, smooth surface of the polymer and the vertical axis shows the observed contact angle for a droplet on the pillared surface of the same type as in Figure 3; the dotted line is a guide to the eye. The pillars are of height 43 µm and so have a roughness factor of r=2.13 complementing the planar solid surface fraction of f=0.196. One way of viewing Figure 4 is that it shows how the liquid repellence due to the chemistry is converted into either a higher degree of repellence or into a greater wetting by the surface structure. Liquids tending towards wetting, such as diidomethane, which form low contact angle droplets on the smooth surface, are entirely drawn into the surface structure on the pillar surface. In contrast liquids tending towards non-wetting, such as glycerol and water, become more non-wetting on the pillar surface.

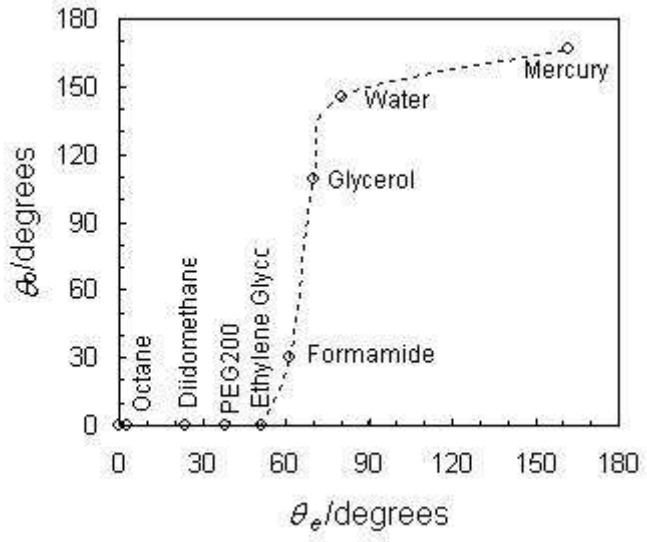

Figure 4 Observed contact angle, θ_o, for droplets of different liquids placed on a surface of type shown in Figure 3 with pillars of height 43 µm; the surface has not had a hydrophobic coating. The results are plotted in sequence using the contact angle, θ_e, measured on the flat polymer surface.

In the description of the skating-to-penetrating transition, we noted that we can use the solid surface fraction, *f*, and the contact angle on the smooth surface to quantitatively predict the contact angles for liquids skating across the pillar surface. For complete penetration of liquids into the surface features, quantitative estimates can also be performed. In this case, theoretical arguments suggest that the effect of the topography is that the cosine of the observed contact angle, $\cos\theta_o$, is a scaling of the cosine of the smooth surface angle by the roughness (Wenzel, 1949). Thus, on the surface in Figure 4, $\cos\theta_o = r\cos\theta_e$, where θ_e is the contact angle on the horizontal axis of Figure 4. Since, the maximum value of $\cos\theta_o$ is unity, and the roughness is greater than one, there is a minimum contact angle θ_e^{min}, below which all liquid droplets spread out into the surface pattern. For the surface in Figure 4, the quantitative estimate is $\cos\theta_o=1$ when $1=2.13\cos\theta_e^{min}$, i.e. $\theta_e^{min}=62^o$, and this is consistent with the data in Figure 4, which show that ethylene glycol and liquids with lower contact angles on the smooth surface are all drawn out into the surface structure and do not form liquid droplets on the pillar surface. These experiments demonstrate that a surface showing extreme water repellence, may, when investigated by liquids other than water or by mixtures including water, such as an MED test, interact with the small scale surface topography via at least two quite different mechanisms (i.e. the penetration-to-skating transition).

Pre-existing Penetration

When a droplet of water sits on a super-hydrophobic material in the skating form, so that water does not penetrate into the pores or gaps between features, we are able to make quantitative estimates of the observed contact angle by imagining the droplet as supported on a composite surface consisting of a surface fraction, *f*, of the solid and a surface fraction (1-*f*) of air. In a similar manner, we can imagine that when there is some pre-existing penetration so that all pores (or gaps) are filled with water, any droplet of water on the surface will then be supported on a composite surface consisting of a surface fraction, *f*, of the solid and a surface fraction (1-*f*) of water (Bico *et al.*, 2001, 2002). In air, a droplet of water completely balls up so that the contact angle is 180^o and $\cos(180^o)=-1$, whereas a droplet of water on a layer of water spreads out completely so that the contact angle is 0^o and $\cos(0^o)=+1$. In these two situations, the observed contact angle can be worked out from the weighted averages of the cosines as $\cos\theta_o = f\cos\theta_e \pm (1-f)$, where the negative sign indicates air in the pores and the positive sign indicates water in the pores. In the former case, the effect is to cause a larger observed contact angle, whereas in the latter case it is to cause a smaller observed contact angle.

As a numerical example of the effect of the pre-existing state of a surface, consider a surface composed of a solid possessing a flat surface contact angle of 90^o formed into a surface with a solid surface fraction $f=0.196$. In this state, the observed contact angle for a droplet of water will be 143.5^o if the pores are filled with air, but only 36.5^o if the pores are filled with water, These considerations suggest that the apparent water repellence of a porous or granular type surface could depend

sensitively on the pre-existing state of the material and whether any of the pores or gaps between grains are filled with water.

Sticky and Slippy Surfaces

The experiments described previously also reveal another aspect of extreme water repellence. Obtaining the image in Figure 1d is difficult because a droplet of water prefers to stay with the syringe rather than detach onto the surface or, if the droplet is mechanically detached and dropped onto the surface, it bounces and, if there is any tilt of the surface, it rolls off. The surface in Figure 1d is both a super-hydrophobic and a slippy surface. In contrast, some super-hydrophobic surfaces are sticky, in the sense that a droplet does not roll away even when a large tilt angle for the surface is applied. Experiments, such as those described by Figure 3, show that the skating droplet corresponds to the slippy surface and the penetrating droplet corresponds to the sticky surface (Quéré *et al*., 2003). It is also worth noting that the previously described surfaces involve solid protrusions which cannot be lifted from the substrate. If grains on a surface are free and sufficiently small then it is energetically preferable for them to attach to the solid-liquid interface and create a completely non-wetting and freely rolling liquid marble (Aussillous and Quéré, 2001; Mahadevan and Pomeau, 1999). Essentially, water itself is sticky even for hydrophobic grains.

SOIL SCIENCE AND SUPER-HYDROPHOBICITY

Super-hydrophobicity

The possible relationship between ideas of super-hydrophobicity in materials science and extreme water repellence in soil science has only occasionally been mentioned in the literature and rarely considered in any depth (Dekker and Ritsema, 2000; Doerr *et al*., 2000; Dekker *et al*., 2005). The requirements for super-hydrophobicity are two-fold: i) the small scale surface topography must be suitable to provide a composite surface of solid and air with gaps or pores small enough that surface tension forces dominate, and ii) the surface chemistry of the solid must be hydrophobic to reduce capillary penetration and must be imparted on the solid without clogging the pores or gaps. What is also clear from experiments is that these conditions can be met in a wide variety of ways. In particular, the surface topography can result from roughness, hairs or fibers, surface texture and porosity, to name just a small number of mechanisms. Whilst this has not been emphasized in the previous section, the skating form of super-hydrophobicity is also favored by surfaces with sharp features. It is therefore a natural question to ask whether the ideas explaining the transformation of the water droplet in Figure 1b to Figure 1c can be applied to the water droplet in Figure 1e and, if so, whether such a transformation might occur naturally in some sandy soils.

Extreme Soil Water Repellence

Reviewing literature on extreme water repellence in soil, at least five reported features appear to suggest a possible relationship to super-hydrophobic materials. First, soil exhibiting extreme water repellence is usually within the upper part of the soil profile (Henry and Paul, 1978; Dekker and Ritsema, 1994), thus suggesting a strong surface effect. Second, it is promoted by drying of soil (DeBano, 2000; Letey, 2001), which would be consistent with water droplets sitting upon a composite solid and air surface. Third, it can be established either via natural processes or oil contamination (Dekker and Ritsema, 2003; Roy and McGill, 1998; 2002), thus indicating that surface chemistry may only need to be of a hydrophobic class rather than a more specific chemistry. Fourth, loose sandy soil is more prone to it (see e.g. the US Fish and Wildlife Service Fuel Effects and Fire Effects Monitoring Guide), although Doerr *et al*., (2000), who also report that that repellency is most commonly observed in sandy soils, note that the highest levels of repellency tends to be reported from medium textured soils, suggesting both a suitable grain size and the existence of gaps between grains. Fifth, forest fires or intense heating of soil is known to cause it by volatilized (hydrophobic) waxes from organic matter, subsequently condensing and coating soil particles (DeBano, 2000; Letey, 2001). This fifth observation is particularly interesting because vapor deposition of a hydrophobic material onto suitable size particles, which are then arranged into a surface, is one way of creating a material with super-hydrophobic properties. A non-soil scientist view could therefore be that soil is a convoluted surface consisting of a porous or granular material coated with hydrophobic compounds and that extreme water repellence occurs when droplets of water bridge between grains and across pores or gaps so that the droplets effectively sit upon a composite solid and air interface. An alternative view incorporating some of these ideas would be that the porous or granular material is less hydrophobic, but is interspersed with hydrophobic grains providing bridging points so that droplets may again adopt a skating configuration.

A Naïve Model of Soil

To quantitatively illustrate how ideas on water repellence might be related to the concept of a super-hydrophobic surface we consider a model of a surface composed of solid spheres (Figure 5a, b) (McHale *et al*., 2005). In this model we assume i) the spheres are of uniform size, ii) the spheres are smooth, iii) the spheres are arranged in a regular, but not necessarily close-packed, pattern, iv) gaps between spheres are small enough for surface tension to be the dominant force, v) droplets of water are gently deposited on the surface rather than grown by condensation onto the surface, vi) if air exists between spheres, the droplets bridge the gap with a horizontal meniscus between the spheres, and vii) the spheres are in fixed locations and cannot be lifted by the surface tension of the water. We also ignore complex grain/pore structure, micro- or macro-aggregates with differing hydrophobicity, water flow and transport properties of soil.

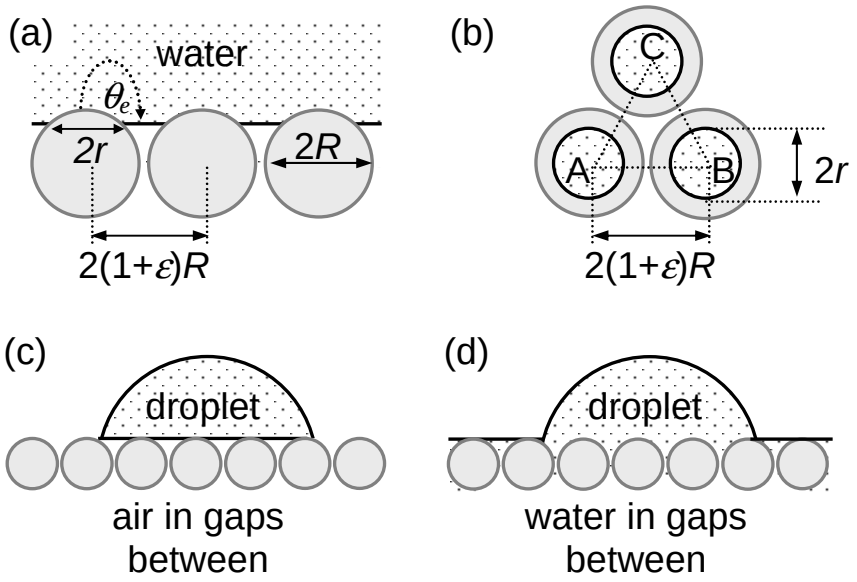

Figure 5 Naive model of substrate composed of solid spheres. (a) side view of packing and hypothesized contact with sphere by water and bridging of air gap by water, (b) top view showing water-solid contact area, (c) droplet sitting on a dry substrate, and (d) droplet sitting on a wet substrate.

Assumptions i)-iii) are clearly an idealized view of grains of sand, but nonetheless capture the idea of the grains providing a solid surface fraction. Modifying assumption i) to include a mixed two size system with the larger size fraction providing the hydrophobic grains could provide a model whereby the water repellence is imparted by micro-aggregates rather than a hydrophobic coating of all grains. It would also be possible to assume that in a mixed size system, the larger grains are in contact with the water and the smaller grains simply extend the distance between larger grains and therefore effectively determine the ε parameter in Figure 5 and the minimum hydrophobicity required to prevent water penetration. Assumption 2 is self-evidently a poor approximation to a typical sandy soil whose grains have sharp asperities. The effect of such asperities will be to increase the intrinsic contact angle needed to prevent penetration of water into the surface, but provided penetration does not occur it will then reduce the fraction of solid surface and so promote water repellence via the Cassie-Baxter mechanism with water bridging grains. If assumption iii) is broken and the grains are not spaced in a regular array, this may create localized areas through which penetration of water occurs and collapses any super-hydrophobic effect; should this not happen then the wider spacing between grains should cause a higher super-hydropobic contact angle. Assumption iv) requires the gaps between grains bridged by water to be substantially less than the capillary length of water of 2.7 mm and so is likely to be valid for particle sizes up to sand, but not for much coarser material. Assumption v) will be true in some situations and not others where pressure forces water into the granular structure. For example, often the skating type configuration for a water droplet is only a metastable one, and growing a droplet by condensation or providing it with an impact force will cause water to penetrate into the surface features and remove any air gaps between grains. Assumption vii), which requires grains to remain in fixed locations, is also likely to be a severe limitation. In

our experiments, we observe that a droplet of water rolled on very fine hydrophobic sand develops a powdery coating and becomes a liquid marble, which is completely non-wetting; the apparent contact angle is then determined by the volume of liquid in the marble and not by the underlying surface on which it rests. A calculation of the free energy change for a hydrophobic grain on the surface to attach to a droplet of water shows it is energetically favorable unless the Young's law contact angle is 180^o- a contact angle that has never been achieved by any surface chemistry (Aussillous and Quéré, 2001). Indeed, if small grains can lift up from the soil due to surface tension, this would be an alternative mechanism to increase water repellency to simply providing a spacing between larger grains. Such a liquid marble is highly mobile on a surface and has implications for run-off and soil erosion. Despite the assumptions and limitations in the model, we believe it is useful to illustrate the effect of a granular hydrophobic surface on water repellence.

To take account of whether the sandy soil prior to droplet deposition is dry or wet we consider the situations shown in Figure 5c and Figure 5d. The first shows a droplet deposited on dry sandy soil and skating across air gaps. The observed contact angle, θ_o^V is then described by the Cassie-Baxter equation for a droplet sitting on a composite solid and air surface,

$$\cos\theta_o^V = f\cos\theta_e - (1-f) \tag{2}$$

where θ_e is the Young's Law contact angle (Eq. (1)) and f is the solid surface area fraction below the droplet. The second shows a droplet deposited on a wet sandy soil with water filling the air gaps. The observed contact angle, θ_o^L is then described by the Cassie-Baxter equation for a droplet sitting on a composite solid and water surface,

$$\cos\theta_o^L = f\cos\theta_e + (1-f) \tag{3}$$

The difference between equations (2) and (3) is in the change in sign of the (1-f) term. This change in sign switches the effect of the space between grains from enhancing water repellence to enhancing wetting. To calculate the observed contact angle taking into account the topography needs knowledge of both the Young's law contact angle θ_e arising from the surface chemistry, and of the solid surface area fraction f. The solid surface fraction f can be worked out from the geometry provided a horizontal meniscus is assumed and this gives,

$$f(\varepsilon) = \frac{1+\cos\theta_e}{1+\cos\theta_e + \dfrac{\sqrt{3}(1+\varepsilon)^2}{\pi} - \dfrac{1}{2}\sin^2\theta} \tag{4}$$

In this calculation, the solid spheres have a radius R and their centre-to-centre separation is $2(1+\varepsilon)R$, where the spacing parameter $\varepsilon>0$ accounts for the fact that the grains are not necessarily close-packed. Full derivation of equations (1)-(4) is given in McHale *et al.* (2005).

To extend consideration of the effect of the separation of the spheres on the model beyond that of previous results, we consider the conditions leading to water penetration into a loose-packed hexagonal bed of spherical grains/spheres where the distance from centre-to-centre of adjacent spheres is $2(1+\varepsilon)R$. Ignoring any hydrostatic pressure, the change in surface free energy ΔF, caused by a layer of water penetrating an extra depth Δh into the upper layer of spheres, when the meniscus is already at a depth h below the top of the spheres in the upper layer, is,

$$\Delta F = -\pi R\gamma_{LV}\left[\cos\theta_e + \left(1-\frac{h}{R}\right)\right]\Delta h \tag{5}$$

The equilibrium depth of penetration, h_e, is then given by,

$$h_e = R\left(1+\cos\theta_e\right) \tag{6}$$

provided the penetrating water does not contact any solid surfaces below the top layer of spheres. Although Eq. (6) does not explicitly depend on the extent of loose packing through the ε parameter this is only because it effectively assumes the upper layer of spheres all rest on a perfectly flat surface through the condition that penetrating water should not contact any solid surfaces from the layer below. In this extreme limit, the maximum penetration is $h_e=2R$ and this corresponds to a minimum Young's law contact angle before water penetrates into the bed of spheres, from Eq. (6), of $\theta_e=0^o$. A more sophisticated view would be to have three adjacent spheres in the upper-most layer forming an equilateral triangle sitting with the central hole they define resting directly on a sphere from the layer beneath. In this case, the minimum Young's law contact angle before penetrating water comes into contact with this sphere from the layer below and induces complete penetration, is given by,

$$\cos\theta_e^{\min} = -1+2\sqrt{\frac{2-2\varepsilon-\varepsilon^2}{3}} \tag{7}$$

Moreover, the maximum ε allowed before the hole between the three spheres is large enough that the sphere below slips through is $\varepsilon_{max}=\sqrt{3}-1=0.732$, which sets a limit on the ε parameter in Eq. (7).When $\varepsilon=0$, the bed of spheres is hexagonal close packed and a layer of water may be supported by solid spheres with $\theta_e>50.73^o$; this is consistent with previous theoretical calculations and experimental data (Bán *et al.*, 1987; Shirtcliffe *et al.*, 2006). Spacing the spheres further apart increases the minimum hydrophobicity needed for water to be suspended by the upper-most layer of spheres and the Cassie-Baxter type super-hydrophobic enhancement to occur, until at $\varepsilon=0.677$ a minimum Young's law contact angle of $\theta_e=120^o$ (around the maximum physically achievable by surface chemistry alone) would be needed to support a layer of water.

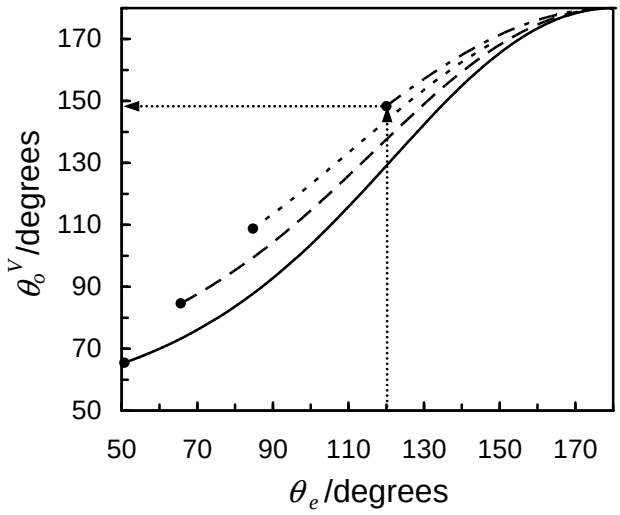

Figure 6 Contact angles, θ_o^V , predicted by the model surface of small spheres with intrinsic hydrophobic contact angles of $\theta_e > \theta_e^{min}$ defined by Eq. (7) and initially possessing air gaps between spheres. The curves ε = 0.0, 0.226, 0.451 and 0.677 show the effect of the spacing between spheres (ε = 0.0 represents close-packing and the arrow shows water repellence increases with spacing of grains).

Figure 6 show results for the model with the ε parameter for the spacing varying from close-packed to loose-packed. The horizontal axis shows the Young's law contact angle, which summarizes the surface chemistry, whilst the vertical axis shows the results of Eq. (2) calculated using Eq. (4) for spacing parameters ε=0.0, 0.226, 0.451 and 0.677. The upper value on ε=0.677 has been chosen because it corresponds to requiring a physically achievable minimum intrinsic (Young's law) contact angle of θ_e=120^o for the Cassie-Baxter effect to occur and a droplet to be suspended by the spherical particles in this model. The solid points at the start of each curve indicate the minimum Young's law contact angle before complete penetration of water into the surface occurs according to Eq. (7). The vertical axis shows the combined effects of surface chemistry and the topography of spheres, either in close packed or loose packed form depending on the value of ε. Figure 6 shows that a surface chemistry with $\theta_e > \theta_e^{min}$ causes a droplet deposited on the dry soil surface (i.e. Figure 5c) to show enhanced water repellence. As ε increases above 0.0 (close-packing) two effects occur. Firstly, the lowest intrinsic contact angle needed to prevent capillary penetration increases systematically. Secondly, for droplets that are suspended by the surface, the enhancement of apparent hydrophobicity, as given by the observed contact angle of a droplet, increases. The dotted arrow in Figure 6 shows that an intrinsic Young's law contact angle of θ_e=120^o will be increased by the Cassie-Baxter effect to θ_e^V=129o, 137^o, 144^o and 148^o for ε=0.0, 0.226, 0.451 and 0.677, respectively.

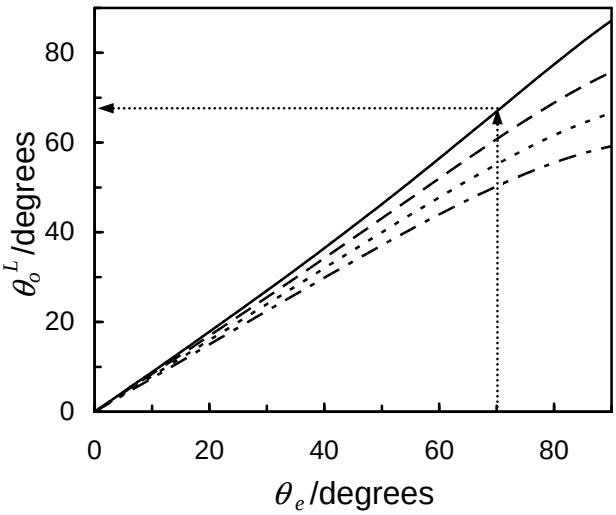

Figure 7 Contact angles, θ_o^L, predicted by the naive model surface of small spheres with intrinsic hydrophobic contact angles of $\theta_e < 90^o$ and initially with water in the gaps between spheres. The curves $\varepsilon = 0.0$, 0.226, 0.451 and 0.677 show the effect of the spacing between spheres ($\varepsilon = 0.0$ represents close-packing and the arrow shows water repellence decreases with spacing of grains).

Figure 7 shows the effects on observed hydrophobicity using the same soil model as in Figure 6, but pre-wet as illustrated in figure 5d. The horizontal axis shows the Young's law contact angle with values less than 90^o, whilst the vertical axes show the results of Eq. (3) calculated using Eq. (4) for spacing parameters ε=0.0, 0.226, 0.451 and 0.677. In this case, no attempt has been made to calculate the affect of a sphere from the layer below the upper-most layer projecting into the space between three spheres in the upper-most layer, because the intention is only to provide a qualitative illustration of the effect of a droplet resting on a composite solid-water surface. As expected from Eq. (3), for any system of solid spheres, the observed contact angle lies between the Young's law contact angle and 0^o and as the spacing between spheres increases the value of observed contact angle reduces. The dotted arrow shows an example with a Young's law contact angle of θ_e=70^o resulting in lower observed contact angles of θ_e^L=67^o, 61^o, 55^o and 50^o, respectively, as the spheres are changed from close-packed (ε=0.0) to loose-packed (ε=0.677).

To examine some of the broad features of the model we conducted experiments using 600 µm and 250 µm nominal diameter glass beads treated with trimethylsilylchloride (TMSCl). Figure 8 shows side profile views of droplets of water on the 600 µm diameter beads (Figure 8a) and the 250 µm diameter beads (Figure 8b). The measured contact angles in these two cases are 126^o and 140^o, respectively, compared to 108^o for a droplet of water on a flat glass surface treated with TMSCl. Whilst the contact angle for droplets on both sizes of beads is larger than on the flat surface, the fact it is different suggests that either the 600 µm diameter

beads are sufficiently large for the assumption that surface tension dominates and droplets bridge the gaps between beads is failing, or that the beads do not pack in a regular close-packed array. This latter conclusion is supported by the fact that Eq. (4) would only predict $f(0)=0.874$ and hence a contact angle increase to 113^o. To obtain a contact angle increase to 140^o, as observed in Figure 8c, would require $f(\varepsilon)=0.339$ with an $\varepsilon=0.807$, although this would be unphysically large for a regular hexagonal model of beads resting on a set of identically sized beads.

Figure 8c shows a top-view of a droplet of water on the 600 µm diameter bead substrate; the droplet is in the centre of the image and acts as a lens to magnify the size of the beads immediately below it. Figure 8d is a view of the 250 µm diameter bead substrate without a droplet of water and at a greater magnification. It is clear that the beads are not in a regular or close-packed arrangement and that the solid surface fraction, f, is much smaller than 0.874, although it is not possible to provide a precise estimate of f from the image. Additional experiments on water droplets on hydrophobic sand grain surfaces have also been presented previously in Figure 1d and Figure 1e. The views of this surface show that its grains have sizes in the 100-400 µm range, that the grains are not close packed and that the grains have sharp asperities. Figure 1e shows an apparent contact angle for water of 139^o, although we believe the angle may be larger as a consequence of the side profile being slightly obscured due to the droplet sitting in a small hollow in the sand. The significance of these experiments with glass beads and hydrophobised sand is not in their precise contact angle results or whether quantitative agreement with the naïve model is obtained, but that simple systems with glass beads of relatively large sizes of 250 µm (and even 600 µm) and fine sand can cause measurable increases in the observed contact angle.

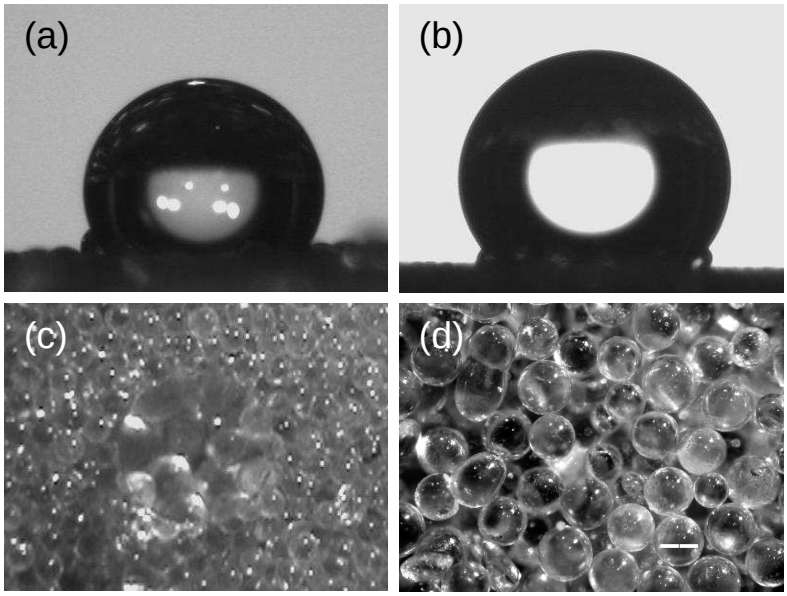

Figure 8 Droplets of water on hydrophobic glass bead substrates. (a) 600 µm diameter beads and a water contact angle of 126^o, (b) 250 µm diameter beads and a water contact angle of 140^o, (c) top view of a droplet of water on the 600 µm diameter bead substrate, and (d) top view of the 250 µm diameter bead substrate.

Close examination of the images from experiments shows that hydrophobic grains can be lifted from the substrate and that the lower surface of a droplet can become coated in a manner similar to a liquid marble (Aussillous and Quéré, 2001). Such liquid marbles are completely non-wetting and highly mobile and could themselves have an impact on soil erosion. Coating liquids with a waxy powder to create liquid marbles is an approach used by galling aphids to remove liquid from inside the plant gall in which they live (Pike *et al.*, 2002). However, this affect could equally easily become a mechanism which erodes loose hydrophobic grains of soil from a surface, cause droplets of water to ball up and increases soil water repellence.

CONCLUSION

In this work we have considered the possible relationship between super-hydrophobic materials and extreme water repellence in soil. A naïve model of spherical close packed spheres has been used to show that large observed contact angles can occur if droplets of water are deposited on such a surface provided it begins in a dry state. For such an enhancement to occur a minimum intrinsic hydrophobicity is required and this increases if the solid spheres are spaced further apart. The model predicts that the same surface, starting in a state with water between the spheres, causes increased wetting rather than extreme water repellence and implies that pre-existing wet soil would reduce water repellence. The model predicts a strong dependence on the separation and packing density of the spheres and this is consistent with experiments using small hydrophobic glass beads and hydrophobic sand. Moreover, these experiments suggest the size range for grains in fine sandy soil is plausible for a super-hydrophobic effect to occur. Such an effect would be consistent with reports of extreme water repellence being related to loose, fluffy, sandy soil. We also suggest that sharp features on sand grains or the microstructure of any wax could have a strong effect on increasing water repellence. An additional mechanism for producing non-wetting, not accounted for in the model and based upon droplets becoming coated in hydrophobic grains, has been identified. Should super-hydrophobic effects be occurring in soil then the molarity of ethanol (MED) droplet test would be a probe of the skating-to-penetrating transition whereas the water droplet penetration time (WDPT) test would investigate droplet penetration routes so that these tests would not necessarily measure the same effects.

ACKNOWLEDGEMENTS

We acknowledge the financial support of the UK Engineering and Physical Sciences Research Council (Grant EP/C509161/1) and the EU-COST Chemistry Action D19, WG-007 and discussions with Dr Stefan Doerr.

REFERENCES

Adamson AW, Gast AP. 1997. Physical Chemistry of Surfaces. John Wiley & Sons, New York.

Aussillous P, Quéré D. 2001. Liquid marbles. *Nature* **411**: 924-927.

Bán S, Wolfram E, Rohrsetzer S. 1987. The condition of starting of liquid imbibition in powders. *Colloids and Surfaces* **22**: 301-309.

Bico J, Thiele U, Quéré D. 2002. Wetting of textured surfaces. *Colloids and Surfaces A* **206**: 41-46.

Bico J, Tordeux C, Quéré D. 2001. Rough wetting. *Europhysics Letters* **55**: 214-220.

Blossey R. 2003. Self-cleaning surfaces – virtual realities. *Nature Materials* **2**: 301–306.

Cassie ABD, Baxter S. 1944. Wettability of porous surfaces. *Transactions of the Faraday Society* **40**: 546–551.

DeBano LF. 2000. The role of fire and soil heating on water repellency in wildland environments: a review. *Journal of Hydrology* **231**: 195–206.

Dekker LW, Ritsema CJ. 1994. How water moves in a water repellent sandy soil .1. Potential and actual water repellency. *Water Resources Research* **30**: 2507-2517.

Dekker LW, Ritsema CJ. 2000. Wetting patterns and moisture variability in water repellent Dutch soils. *Journal of Hydrology* **231**: 148-164.

Dekker LW, Ritsema CJ (Eds). 2003. Soil water repellency: Origin, consequences and amelioration. Elsevier, Amsterdam.

Dekker LW, Oostindie K, Ritsema CJ. 2005. Exponential increase of publications related to soil water repellency. *Australian Journal of Soil Research* **43**: 403-441.

Doerr SH. 1998. On standardizing the 'water drop penetration time' and the 'molarity of an ethanol droplet' techniques to classify soil hydrophobicity: a case study using medium textured soils. *Earth Surface Processes and Landforms* **23**: 663–668.

Doerr SH, Shakesby RA, Walsh RPD. 2000. Soil water repellency: its causes, characteristics and hydro-geomorphological significance. *Earth-Science Reviews* **51**: 33-65.

Doerr SH, Ferreira AJD, Walsh RPD, Shakesby RA, Leighton-Boyce G, Coelho COA. 2003. Soil water repellency as a potential parameter in rainfall-runoff modelling: experimental evidence at point to catchment scales from Portugal. *Hydrological Processes* **17**: 363-377.

Fox DM, Darboux F, Carrega P. 2007. Effects of fire-induced water repellence on soil aggregate stability, splash erosion and saturated hydraulic conductivity for different size fractions. *Hydrological Processes* **21:** 2377–2384.

Henry JM, Paul JL. 1978. Hydrophobic soils on putting greens. *California Turfgrass Culture* **28**: 9–11.

Karnok KA, Rowland EJ, Tan KH. 1993. High ph treatments and the alleviation of soil hydrophobicity on golf greens. *Agronomy Journal* **85**: 983-986.

Letey J. 2001. Causes and consequences of fire-induced soil water repellency. *Hydrological Processes* **15**: 2867–2875.

Mahadevan L, Pomeau Y. 1999. Rolling droplets. *Physics of Fluids* **11**: 2449-2453.

McHale G, Newton MI, Shirtcliffe NJ. 2005. Water-repellent soil and its relationship to granularity, surface roughness and hydrophobicity: a materials science view. *European Journal of Soil Science* **56**: 445-452.

Pike N, Richard D, Foster W, Mahadevan L. 2002. How aphids lose their marbles. *Proceedings of the Royal Society of London* **B269**: 1211-1215.

Quéré D, Lafuma A, Bico J. 2003. Slippy and sticky microtextured solids. *Nanotechnology* **14**: 1109–1112.

Roy JL, McGill WB. 1998. Characterization of disaggregated nonwettable surface soils found at old crude oil spill sites. *Canadian Journal of Soil Science* **78**: 331-344.

Roy JL, McGill WB. 2002. Assessing soil water repellency using the molarity of ethanol droplet (MED) test. *Soil Science* **167**: 83-97.

Shirtcliffe NJ, McHale G, Newton MI, Pyatt FB, Doerr SH. 2006. Critical conditions for the wetting of soils. *Applied Physics Letters* **89**: Art. No. 094101.

Shirtcliffe NJ, McHale G, Newton MI, Perry CC. 2005a. Wetting and wetting transitions on copper-based super-hydrophobic surfaces. *Langmuir* **21**: 937-943.

Shirtcliffe NJ, McHale G, Newton MI, Perry CC, Roach P. 2005b. Porous materials show superhydrophobic to superhydrophilic switching. *Chemical Communications* **25**: 3135-3137.

Shirtcliffe NJ, McHale G, Newton MI, Perry CC. 2003. Intrinsically superhydrophobic organosilica sol-gel foams. *Langmuir* **19**: 5626-5631.

Shirtcliffe NJ, Aqil S, Evans C, McHale G, Newton MI, Perry CC, Roach P. 2004. The use off high aspect ratio photoresist (SU-8) for super-hydrophobic pattern prototyping. *Journal of Micromechanical and Microengineering* **14**: 1384-1389.

Terry JP, Shakesby RA. 1993. Soil hydrophobicity effects on rainsplash – simulated rainfall and photographic evidence. *Earth Surface Processes and Landforms* **18**: 519–525.

Van't Woudt BD. 1959 Particle coatings affecting the wettability of soils. Journal of *Geophysical Research* **64**: 263-267.

Wenzel RN. 1949. Surface roughness and contact angle. *Journal of Physical and Colloid Chemistry* **53**: 1466–1467.

FIGURE CAPTIONS

Figure 1 Side view profiles of water droplets and their reflections on (a) a flat copper surface, (b) a flat hydrophobic copper surface, and (c) a hydrophobized etched copper surface. Panel (d) shows the packing and density of a surface composed of hydrophobic sand (scale bar is 200 μm), and (e) shows a droplet of water (contact angle of 139^o) on the surface in (d).

Figure 2 Skating-to-penetrating transition on a hydrophobic foam. (a) Droplet of water with some food coloring on an MTEOS sol-gel, (b) same sol-gel, but after heat treatment to remove the hydrophobic surface functional groups: the droplet of water completely penetrates and stains the foam. (c) the pore structure of the sol-gel used in (a) and (b).

Figure 3 Observed contact angle, θ_o, for a water droplet on square lattices of polymer pillars of diameter 15 μm and centre-to-centre separation of 30 μm and various heights; the surface has been treated with a hydrophobic coating. The inset shows an SEM image of the surface.

Figure 4 Observed contact angle, θ_o, for droplets of different liquids placed on a surface of type shown in Figure 3 with pillars of height 43 μm; the surface has not had a hydrophobic coating. The results are plotted in sequence using the contact angle, θ_e, measured on the flat polymer surface.

Figure 5 Naive model of substrate composed of solid spheres. (a) side view of packing and hypothesized contact with sphere by water and bridging of air gap by water, (b) top view showing water-solid contact area, (c) droplet sitting on a dry substrate, and (d) droplet sitting on a wet substrate.

Figure 6 Contact angles, θ_o^V , predicted by the model surface of small spheres with intrinsic hydrophobic contact angles of $\theta_e > \theta_e^{min}$ defined by Eq. (7) and initially possessing air gaps between spheres. The curves $\varepsilon = 0.0$, 0.226, 0.451 and 0.677 show the effect of the spacing between spheres ($\varepsilon = 0.0$ represents close-packing and the arrow shows water repellence increases with spacing of grains).

Figure 7 Contact angles, θ_o^L, predicted by the naive model surface of small spheres with intrinsic hydrophobic contact angles of $\theta_e < 90^o$ and initially with water in the gaps between spheres. The curves $\varepsilon = 0.0$, 0.226, 0.451 and 0.677 show the effect of the spacing between spheres ($\varepsilon = 0.0$ represents close-packing and the arrow shows water repellence decreases with spacing of grains).

Figure 8 Droplets of water on hydrophobic glass bead substrates. (a) 600 µm diameter beads and a water contact angle of 126^{o}, (b) 250 µm diameter beads and a water contact angle of 140^{o}, (c) top view of a droplet of water on the 600 µm diameter bead substrate, and (d) top view of the 250 µm diameter bead substrate.

FIGURES

Figure 1 Side view profiles of water droplets and their reflections on (a) a flat copper surface, (b) a flat hydrophobic copper surface, and (c) a hydrophobized etched copper surface. Panel (d) shows the packing and density of a surface composed of hydrophobic sand (scale bar is 200 µm), and (e) shows a droplet of water (contact angle of 139^{o}) on the surface in (d).

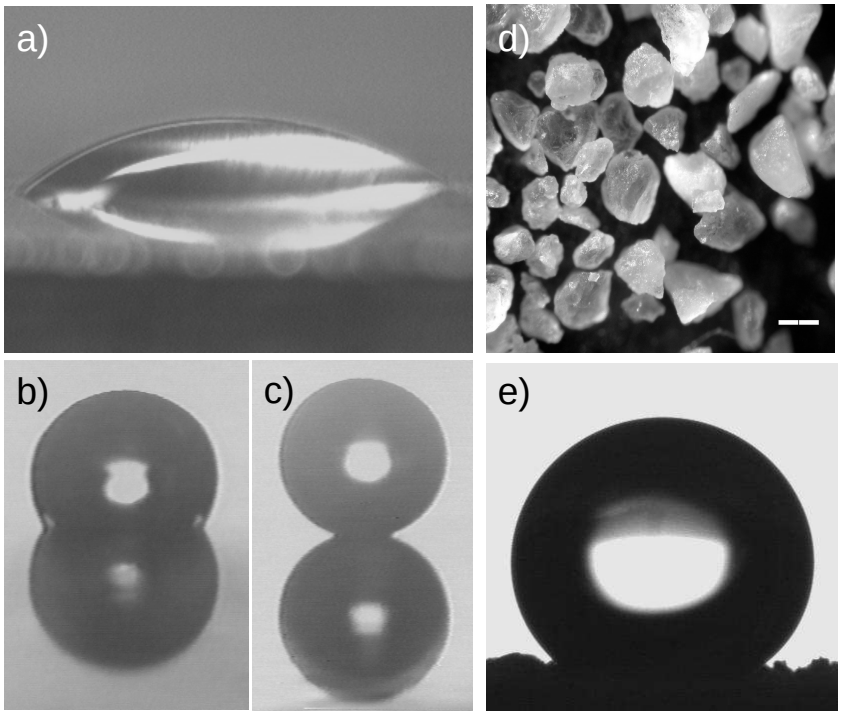

Figure 2 Skating-to-penetrating transition on a hydrophobic foam. (a) Droplet of water with some food coloring on an MTEOS sol-gel, (b) same sol-gel, but after heat treatment to remove the hydrophobic surface functional groups: the droplet of water completely penetrates and stains the foam. (c) the pore structure of the sol-gel used in (a) and (b) (scale bar is 10 µm).

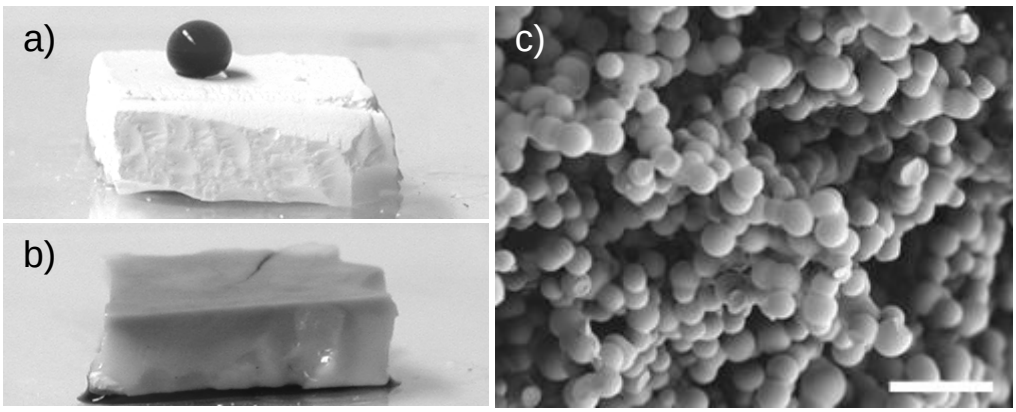

Figure 3 Observed contact angle, θ_o, for a water droplet on square lattices of polymer pillars of diameter 15 µm and centre-to-centre separation of 30 µm and various heights; the surface has been treated with a hydrophobic coating. The inset shows an SEM image of the surface.

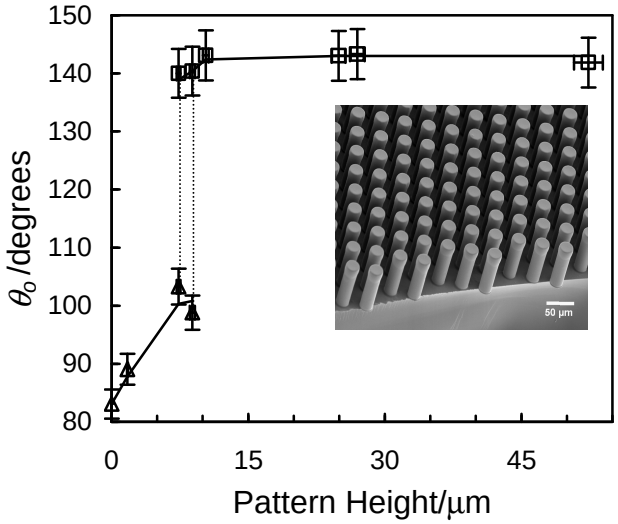

Figure 4 Observed contact angle, θ_o, for droplets of different liquids placed on a surface of type shown in Figure 3 with pillars of height 43 µm; the surface has not had a hydrophobic coating. The results are plotted in sequence using the contact angle, θ_e, measured on the flat polymer surface.

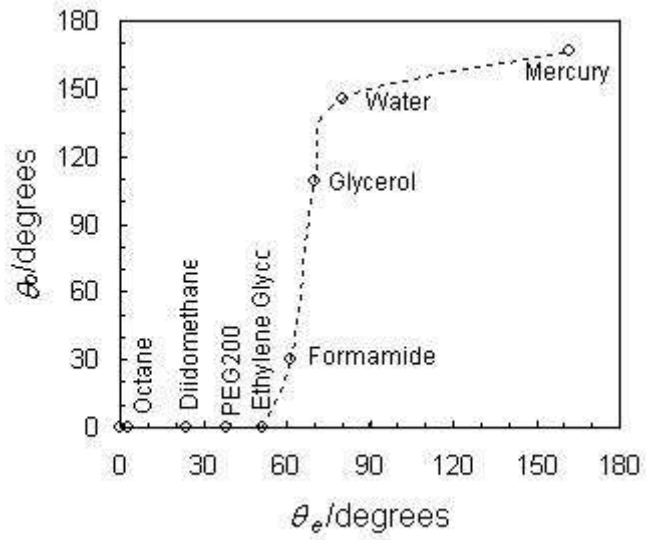

Figure 5 Naive model of substrate composed of solid spheres. (a) side view of packing and hypothesized contact with sphere by water and bridging of air gap by water, (b) top view showing water-solid contact area, (c) droplet sitting on a dry substrate, and (d) droplet sitting on a wet substrate.

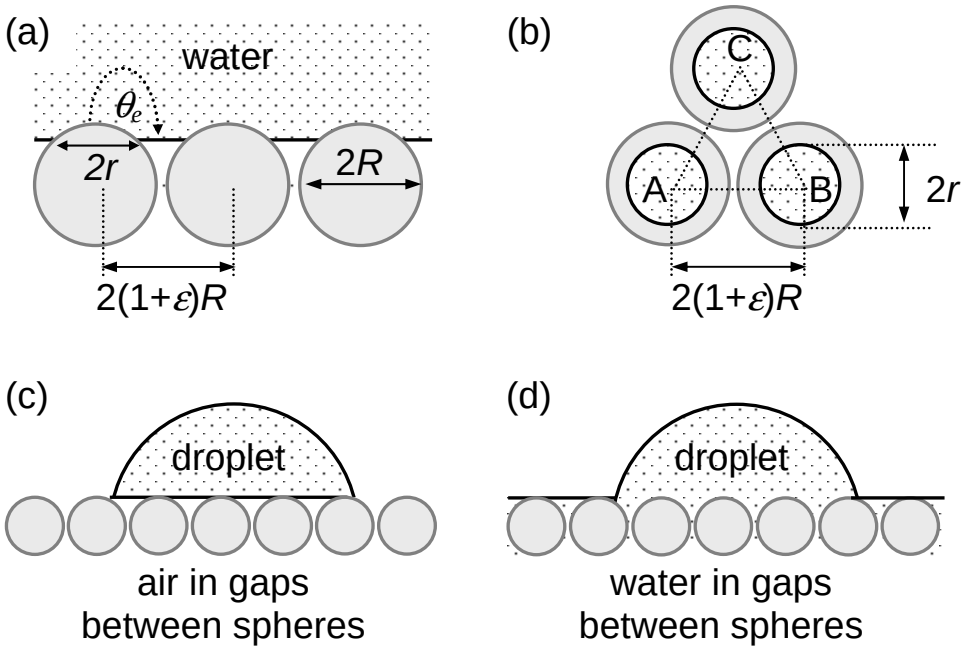

Figure 6 Contact angles, θ_o^V , predicted by the model surface of small spheres with intrinsic hydrophobic contact angles of $\theta_e > \theta_e^{min}$ defined by Eq. (7) and initially possessing air gaps between spheres. The curves $\varepsilon = 0.0$, 0.226, 0.451 and 0.677 show the effect of the spacing between spheres ($\varepsilon = 0.0$ represents close-packing and the arrow shows water repellence increases with spacing of grains).

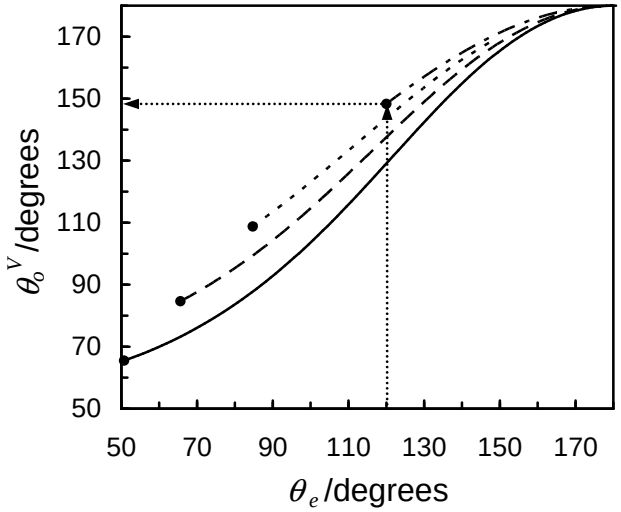

Figure 7 Contact angles, θ_o^L, predicted by the naive model surface of small spheres with intrinsic hydrophobic contact angles of $\theta_e < 90^o$ and initially with water in the gaps between spheres. The curves $\varepsilon = 0.0$, 0.226, 0.451 and 0.677 show the effect of the spacing between spheres ($\varepsilon = 0.0$ represents close-packing and the arrow shows water repellence decreases with spacing of grains).

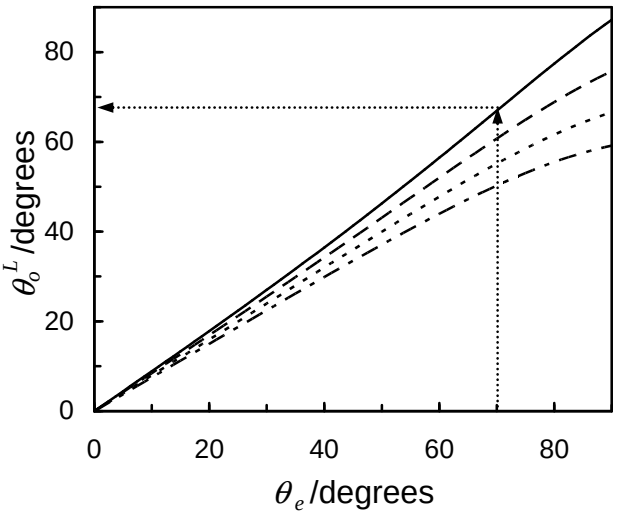

Figure 8 Droplets of water on hydrophobic glass bead substrates. (a) 600 µm diameter beads and a water contact angle of 126^o, (b) 250 µm diameter beads and a water contact angle of 140^o, (c) top view of a droplet of water on the 600 µm diameter bead substrate, and (d) top view of the 250 µm diameter bead substrate.